INTERNATIONAL JOURNAL FOR NUMERICAL METHODS IN FLUIDS, VOL. 4, 159–170 (1984)

BOUNDARY INTEGRAL EQUATION METHOD FOR SOME STOKES PROBLEMS

HÜSNÜ TÖZEREN

Department of Engineering Sciences, Middle East Technical University, Ankara, Turkey

SUMMARY

The boundary integral equation method is a numerical technique extensively applied in the solution of boundary value problems from many different engineering fields. The starting point of the method is the formulation of an integral equation which gives the variable at any point in terms of single and double layer potentials whose densities are the values of the variable and its derivatives on the boundary. The method consists of the numerical solution of this integral equation when the field point is taken to lie on the boundary. The present paper extends the formulation of the method to Stokes flows of a collection of particles in infinite circular cylinders. This is achieved by developing matrix Green's functions for Stokes flows in cylindrical boundaries. The results are found to be in good agreement with the results of Wang and Skalak[1] and Tözeren.[3]

KEY WORDS Boundary Method Green's Function Stokes Flow Cylindrical Tubes Collections of Particles

1. INTRODUCTION

The slow viscous flow past a collection of particles is of interest in many engineering fields and has received considerable study.[3] For particles of some special shapes, analytic solutions have been derived by applying separation of variables to Stokes equations. Some examples are the series solution in spherical co-ordinates as given by Lamb[4] and series in bi-spherical co-ordinates used by Stimson and Jeffery[5] and Tözeren and Skalak[6] in the interactions of two spheres.

The two most extensively used numerical techniques are (i) boundary solution procedures based on solutions of Stokes equations satisfying boundary conditions only approximately and (ii) the method of reflections, an iterative procedure. In the study of multiparticle configurations, boundary methods have very successful applications.[7] The method of reflections, until recently the most popular technique, is very slowly convergent when the particle spacing and the distance from particles to boundaries are comparable to the dimensions of the particles.

As opposed to the techniques mentioned above, finite elements and finite differences are applicable for particles of arbitrary shapes. Many boundary value problems in infinite domains are solved using these techniques in conjunction with boundary solution procedures. Zienkiewicz, Kelly and Bettess[8] discuss some applications in flow in porous media, heat conduction and wave propagation in which the finite elements are introduced in some bounded (interior) region and boundary solution procedures are applied in the unbounded (exterior) region. The additional parameters of the boundary solution procedures are eliminated by using the continuity conditions at the common boundary. (These applications show that the finite element and finite difference formulations can be generalized to

0271–2091/84/020159–12$01.20

Received 26 March 1982
Revised 25 November 1982

unbounded Stokes flow problems readily in contrast to the remarks by Leichtberg *et al.*[7] and Youngren and Acrivos.[9])

Another numerical technique recently applied to Stokes flow problems is the boundary integral equation method.[10,11] Using this method, Youngren and Acrivos[9] studied the Stokes flow past particles of a variety of different shapes. The starting point of their work is the formulation of an integral equation (the Green's formula for Stokes equations) which gives velocities at any point in terms of velocities and stresses on the particle surface. The method consists of the numerical solution of this integral equation when the field point is taken to lie on the boundary.

This paper presents a formulation of the boundary integral equation method for axisymmetric slow viscous flow past a collection of particles in a circular cylindrical tube. The boundary integral equation corresponding to the Stokes problem is given in Section 2. This formula involves integrals taken along the surface of particles and the circular cylindrical surface. However, the integrals along the infinite cylindrical surface vanish if the matrix Green's function is used in place of Stokeslet solutions in the boundary integral equation. Liron and Shahar[12] give the Green's functions for the general three dimensional case. A similar approach valid for axisymmetric configurations is outlined in Section 3. Extensive numerical tests are performed and the results on flow of spherical or spheroidal particles and a pair of spherical particles are compared with the results of previous work in Section 4.

2. BOUNDARY INTEGRAL EQUATION

Consider the Poiseuille flow past a particle of arbitrary shape in an infinite circular cylinder (Figure 1). The equations governing the motion are the Stokes equations and equation of continuity:

$$\mu \nabla^2 \mathbf{v} = \operatorname{grad} p, \qquad \operatorname{div} \mathbf{v} = 0 \tag{1}$$

where μ is the viscosity of the fluid and p is pressure. The disturbance velocity $\mathbf{v}$ is subject to the following boundary conditions:

$$\begin{aligned} &\mathbf{v}(x) = \mathbf{k}\left[U - V\left(1 - \frac{r^2}{r_0^2}\right)\right], \qquad x \in S_P \\ &\mathbf{v}(x) = 0, \qquad x \in S_T, \qquad \mathbf{v} \to 0 \quad \text{as} \quad z \to \mp\infty. \end{aligned} \tag{2}$$

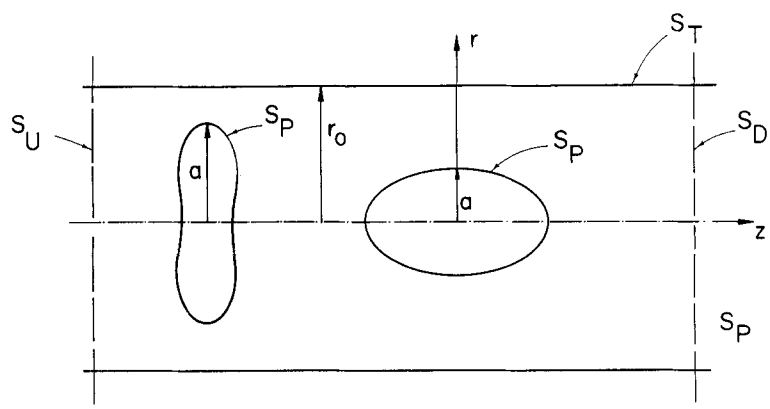

Figure 1. Axisymmetric slow viscous flow past particles of arbitrary shape in an infinite circular cylinder

where U and $V/2$ are the particle and average velocities; S_p, S_T are the particle surface and the surface of the tube respectively; and $\mathbf{k}$ is the unit vector in the z direction.

A solution of (1) in terms of potentials of single and double layers is given by Ladyzhenskaya[13] (see also Reference 9):

$$v_k(x) = \int_S T'_{ij}(\mathbf{u}^k(x, y))_y v_i n_j \, dS - \int_S u^i_k(x, y)\sigma_{ij}(\mathbf{v})n_j \, dS \tag{3}$$

where $\sigma_{ij}(\mathbf{v})$ is the stress tensor for velocities v_i, u^i_k is the fundamental singular solution of Stokes equations (a Stokeslet) and $T'_{ij}(u^k(x, y)_y$ is the stress tensor given by equations (3.5) and (3.11) of Reference 13.

$$u^k_j(x, y) = -\frac{1}{8\pi\mu}\left[\frac{\delta^k_j}{|x-y|} + \frac{(x_j - y_j)(x_k - y_k)}{|x-y|^3}\right]$$

$$q^k(x, y) = -\frac{x_k - y_k}{4\pi\,|x-y|^3} \tag{4}$$

and

$$T'_{ij}(\mathbf{u}^k) = \delta^i_j q(x, y) + \mu\left(\frac{\partial u^k_i(x, y)}{\partial y_j} + \frac{\partial u^k_j(x, y)}{\partial y_i}\right); \qquad i, j, k = 1, 2, 3,$$

where x is an arbitrary field point, y is the point of application of Stokeslet, δ^i_j is the Kronecker delta and $|x-y|$ is the distance between the points x and y.

The singular surface integrals in (3) along the infinite cylindrical surface can be eliminated by using the matrix Green's functions G^k_j, g^k in place of the Stokeslet solution. The G^k_j and g^k are defined by the solution of the following equations:

$$\mu\,\nabla^2_x G^k_j(x, y) = \frac{\partial}{\partial x_j} g^k(x, y)$$

$$\frac{\partial}{\partial x_i} G^k_i = 0 \quad \text{everywhere except } x = y$$

and

$$G^k_i = 0 \quad \text{at } S_T \text{ for } i, j, k = 1, 2, 3. \tag{5}$$

Equation (3) written for $u^k_j = G^k_j$ and the surface $S = S_p + S_T + S_U + S_D$ is (where S_U and S_D are upstream and downstream faces as shown in Figure 1)

$$v_k(x) = \int_{S_p} T'_{ij}(\mathbf{G}^k)v_i n_j \, dS - \int_{S_p} G^i_k \sigma_{ij}(\mathbf{v})n_j \, dS \tag{6}$$

The integrals along S_T, S_U and S_D vanish since $G^i_j = v_j = 0$ for $x \in S_T$ and G^i_j, $v_i \to 0$ as $z \to \mp\infty$.

It is possible to simplify the equation (6) even further by applying Green's formula (equation 2.5 in Reference 9 and equation 3.10 of Reference 13) to the flow

$$\mathbf{v} = \mathbf{u} = \mathbf{k}\left[U - V\left(1 - \frac{r^2}{r_0^2}\right)\right], \qquad \sigma_{ij}(v) = \tau_{ij}(\mathbf{u})$$

in the region bounded by the particle surface (where τ_{ij} are stresses due to Poiseuille flow):

$$0 = \int_S T'_{ij}(\mathbf{G}^k)u_i n_j \, dS - \int_{S_p} G^i_k \tau_{ij}(\mathbf{u})n_j \, dS \tag{7}$$

Subtraction of (7) from (6) and use of $u_i = v_i$ at $y \in S_T$ lead to an expression for $v_k(x)$ in terms of single layer potentials alone:

$$v_k(x) = -\int_{S_p} G_k^i(x, y)(\sigma_{ij}(\mathbf{v}) - \tau_{ij}(\mathbf{u}))n_j \, dS \tag{8}$$

The density $f_i = (\sigma_{ij}(\mathbf{v}) - \tau_{ij}(\mathbf{u}))n_j$ of the kernel G_k^i is the difference of traction components of the actual flow and Poiseuille flow at S_p.

For axisymmetric flows the dimension of the problem is reduced:

$$\begin{aligned} v_z &= -\int_{C_p} (G_z^r f_r + G_z^z f_z) \, ds \\ v_r &= -\int_{C_p} (G_r^r f_r + G_r^z f_z) \, ds \end{aligned} \tag{9}$$

where ds is infinitesimal arclength and C_p is the generating arc of the surface S_p. The $\mathbf{G}^r$ and $\mathbf{G}^z$ are Green's functions which correspond to the singular solutions for the force fields $1/r'^2 \, \delta(r - r') \, \delta(\cos\theta - \cos\theta')\mathbf{e}^r$ and $1/r'^2 \, \delta(r - r') \, \delta(\cos\theta - \cos\theta')\mathbf{e}^z$ (distribution of Stokeslets in r and z directions on the rings around the symmetry axis, $r = r'$ and $\theta = \theta'$).

Knowing the velocities v_r and v_z on the surface, equation (9) can be solved for the density f_i by transforming this integral equation into a system of algebraic equations.[9] This is achieved by dividing C_p into a number of elements, introducing unknown tractions at each node, assuming f_i varies linearly within each element and carrying out the integrals in (9) of the terms multiplied by the nodal values of f_i numerically.

In the next section, the matrix Green's function for axisymmetric Stokes problems in an infinite circular cylinder is developed by using the Fourier transform technique.

3. GREEN'S FUNCTION

In order to handle Stokes problems in infinite circular cylinders by the boundary integral equation method it is necessary to determine Green's function for cylindrical boundaries. This is obtained by Liron and Shahar[9] for the general three dimensional flow. In this section, using Fourier transforms, the Green's function G_j^i is developed in the particular case of axisymmetric flow.

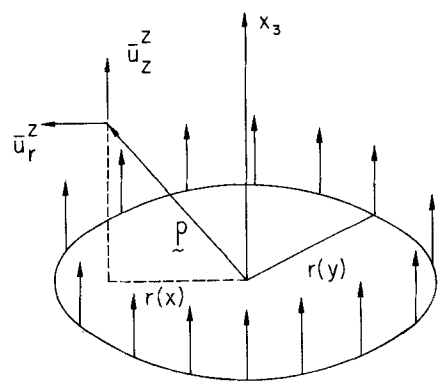

Figure 2. The velocity $\bar{\mathbf{u}}^z$ at position $\mathbf{p} = (r(x), z)$ due to a ring-like distribution of Stokeslets in the axial direction at $(r(y), 0)$

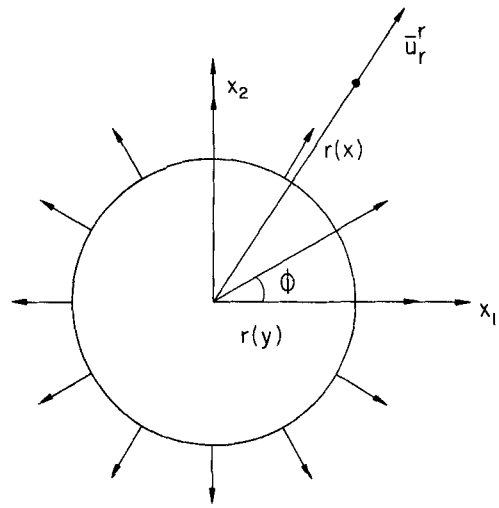

Figure 3. The velocity $\bar{\mathbf{u}}^r$ due to a ring of Stokeslets in the radial direction

The axisymmetric Green's function has the same type of singularity as the velocity field due to a ring of Stokeslets $\bar{u}_j^i$ (such rings of Stokeslets in the z and r directions are illustrated in Figures 2 and 3). The $\bar{u}_j^i$ given below are obtained by integration of certain u_j^i components with respect to the azimuthal angle ϕ:

$$\begin{aligned}
\bar{u}_z^z &= -\frac{1}{4\pi\mu} kr(x)^{-1/2} r(y)^{-1/2} \left\{ K(k) + \frac{z^2}{r_{xy}^2} E(k) \right\} \\
\bar{u}_r^z &= -\frac{z}{8\pi\mu} kr(x)^{-3/2} r(y)^{-1/2} \left\{ K(k) + (r(x)^2 - r(y)^2 - z^2) \frac{E(k)}{r_{xy}^2} \right\} \\
\bar{u}_z^r &= \frac{1}{8\pi\mu} kzr(y)^{-3/2} r(x)^{-1/2} \left\{ K(k) - (r(x)^2 - r(y)^2 + z^2) \frac{E(k)}{r_{xy}^2} \right\} \\
\bar{u}_r^r &= -\frac{1}{8\pi\mu} kr(x)^{-3/2} r(y)^{-3/2} \left\{ (r(x)^2 + r(y)^2 + 2z^2) K(k) \right. \\
&\quad \left. - (2z^4 + 3(r(x)^2 + r(y)^2) z^2 + (r(x)^2 - r(y)^2)^2) \frac{E(k)}{r_{xy}^2} \right\}
\end{aligned} \tag{10}$$

where $k = \dfrac{2\sqrt{[r(x)r(y)]}}{\sqrt{[z^2 + (r(x) + r(y))^2]}}$, $r_{xy}^2 = |x - y|$ and $K(k)$ and $E(k)$ are complete elliptic integrals of first and second kinds.

Although they have the same singular behaviour as G_j^i the velocities $\bar{u}_j^i$ violate the no-slip boundary condition on S_T. Finding a regular solution of Stokes equations which has equal but opposite boundary values at S_T and superposing $\bar{u}_j^i$ with this solution yields the axisymmetric Green's function.

The general axisymmetric solution of Stokes equations in cylindrical co-ordinates is

$$\begin{aligned}
v_z &= \int_0^\infty [tI_0(rt)A(t) + (rtI_1(rt) + 2I_0(rt))B(t)] \cos zt \, dt \\
v_r &= \int_0^\infty [tI_1(rt)A(t) + rtI_0(rt)B(t)] \sin zt \, dt
\end{aligned} \tag{11}$$

for v_z = even, v_r = odd with respect to z, and

$$\begin{aligned} v_z &= \int_0^\infty [tI_0A(t) + (rtI_1 + 2I_0)B(t)] \sin zt \, dt \\ v_r &= -\int_0^\infty [tI_1A(t) + rtI_0B(t)] \cos zt \, dt \end{aligned} \tag{12}$$

for v_z = odd and v_r = even, where I_0 and I_1 are modified Bessel functions of zero and first orders. The functions $A(t)$ and $B(t)$ must be so chosen that the regular solution (v_z, v_r) satisfies the boundary condition $v_j^i = -\bar{u}_j^i$ at the tube surface, $r(x) = r_0$. This is possible if the expressions within the square brackets in (11) and (12) are equal to the Fourier transforms of $-\bar{u}_j^i$ at $r = r_0$. The $\bar{u}_j^i$ for fixed $r(x) = r_0$ can be written as inverse Fourier transforms (cosine transform for even functions, sine for odd) by using equations (7.3.38)–(7.3.41) of Reference 3:

$$\begin{aligned} \bar{u}_j^i(r_0, z; r(y), 0) &= \int_0^\infty g_j^i(t) \cos zt \, dt \\ &= \int_0^\infty g_j^i(t) \sin zt \, dt \end{aligned} \tag{13}$$

where

$$\begin{aligned} g_z^z &= -\frac{1}{2\pi\mu}[2K_0(r_0t)I_0(rt) - r_0tK_1(r_0t)I_0(rt) + rtK_0(r_0t)I_1(rt)] \\ g_z^r &= \frac{1}{2\pi\mu}[rtK_1(r_0t)I_1(rt) - r_0tK_0(r_0t)I_0(rt)] \\ g_z^r &= -\frac{1}{2\pi\mu}[r_0tK_1(r_0t)I_1(rt) - rtK_0(r_0t)I_0(rt)] \\ g_r^r &= -\frac{1}{2\pi\mu}[2K_1(r_0t)I_1(rt) + r_0tK_0(r_0t)I_1(rt) - rtK_1(r_0t)I_0(rt)] \end{aligned} \tag{14}$$

and

$$r = r(y) \quad \text{and} \quad r(x) = r_0.$$

The conditions $v_j^i = -\bar{u}_j^i$ at $r = r_0$ can be written as

(i) for ring-like distribution of Stokeslets in the z direction

$$\begin{aligned} tI_0(r_0t)A(t) + (r_0tI_1(r_0t) + 2I_0(r_0t))B(t) &= -g_z^z \\ tI_1(r_0t)A(t) + r_0tI(r_0t)B(t) &= -g_r^z \end{aligned} \tag{15}$$

(ii) for a ring of Stokeslets in the r direction

$$\begin{aligned} tI_0(r_0t)A(t) + (r_0tI_1(r_0t) + 2I_0(r_0t))B(t) &= -g_z^r \\ -tI_1(r_0t)A(t) - r_0tI_0(r_0t)B(t) &= -g_r^r(t) \end{aligned} \tag{16}$$

Solving for the functions $A(t)$ and $B(t)$ from these equations; substituting into equations (11) and (12) and carrying out the integrals in t gives the regular solutions v_j^i as functions of $r(x)$, $r(y)$ and z. Finally, the superposition of v_j^i with $-\bar{u}_j^i$ yield the Green's functions G_j^i.

4. NUMERICAL RESULTS

For numerical solution of the boundary integral equation (9) the curve C_p is subdivided into a number of elements and an unknown traction vector (f_r^n, f_z^n) is introduced associated with each node. The components of traction f_r and f_z are assumed to vary linearly within each element (see Reference 14 for linear and higher order elements in boundary element techniques):

$$f_i(x) = f_i^1 N_1(x) + f_i^2 N_2(x) \tag{17}$$

where $N_1(x)$ and $N_2(x)$ are linear shape functions. Using (17), equation (9) is replaced by the approximate boundary integral equation

$$v_z(x) = -\sum_{n=1}^{n_e} \left\{ f_r^n \int_{C_n} G_z^r(x, y) N_1(y)\, ds + f_r^{n+1} \int_{C_n} G_z^r(x, y) N_2(y)\, ds \right.$$
$$\left. + f_z^n \int_{C_n} G_z^z(x, y) N_1(y)\, ds + f_z^{n+1} \int_{C_n} G_z^z(x, y) N_2(y)\, ds \right\} \tag{18}$$

where n_e is the total number of elements and C_n is the element n. Substitution of known values of $\mathbf{v}$ at (n_e+1) different points and computing the integrals within each element transform the integral equation into a set of linear equations for the unknowns, nodal traction components.

The axisymmetric fundamental solution (10) is not valid for the nodes on the symmetry axis, $r(y) = 0$. However, taking limits of these expressions as $r(y) \to 0$ we obtain well defined velocity components for any point $r(x) \neq r(y)$, $z \neq 0$ using the limiting behaviours of k, K, E $\left(k \sim r(y)^{1/2},\ K \sim \frac{\pi}{2}(1+\frac{1}{4}k^2) \text{ and } E \sim \frac{\pi}{2}(1-\frac{1}{4}k^2) \text{ as } r(y) \to 0\right)$. These simplified expressions can then be used in equation (18) for the nodes on the symmetry axis in place of fundamental solution (10). It is found easier to carry out this limiting procedure numerically

Table I. Velocities at $z = 0{\cdot}0, r = 1{\cdot}0$ due to rings of Stokeslets (r', z'). Comparison of exact values with Fourier transforms numerically integrated using different N = number of steps and T = integration limit

Location of Stokeslet	N	T	Velocities v_z^z	v_r^z	v_z^r	v_r^r
	Exact		0·251878	0·001207	0·024805	0·011986
$r' = 0{\cdot}1$	600	50·0	0·251882	0·001207	0·024805	0·011986
$z' = 0{\cdot}1$	400	50·0	0·251885	0·001207	0·024806	0·011986
	200	50·0	0·251938	0·001207	0·024808	0·011987
	200	25·0	0·251891	0·001207	0·024809	0·011987
	Exact		0·27134	0·006796	0·081277	0·016556
$r' = 0{\cdot}3$	600	50·0	0·27135	0·006796	0·081287	0·016556
$z' = 0{\cdot}4$	400	50·0	0·27135	0·006796	0·081280	0·016557
	200	25·0	0·27136	0·006795	0·081282	0·016558
	Exact		0·27088	0·016158	0·073243	0·011372
$r' = 0{\cdot}6$	600	50·0	0·27085	0·016138	0·07327	0·011317
$z' = 0{\cdot}9$	400	50·0	0·27090	0·016165	0·073245	0·011385
	200	25·0	0·27090	0·016163	0·073256	0·011369

Table II. The coefficients of additional drag λ_U and λ_V computed using different values of T and N (total number of elements, $n_e = 10$ and order of Gaussian quadrature, $m = 5$ for all cases)

		$a/r_0 = 0{\cdot}5$		$a/r_0 = 0{\cdot}7$	
N	T	λ_U	λ_V		
600	50	5·9414	4·9860	24·265	17·137
400	50	5·9414	4·9860	24·268	17·139
200	50	5·9439	4·9881	24·380	17·217
200	25	5·9416	4·9861	24·253	17·128

by testing the convergence of relevant integrands in (18) taking $r(y) = 10^{-3}, 10^{-4}, 10^{-5}, \ldots$. Three iterations at most was sufficient to obtain six significant figures.

Various tests are performed to determine the accuracy of this procedure compared to other numerical methods. In all these tests, the element lengths are chosen to be equal. The line integrals within each element (18) are calculated using Gaussian quadratures. If the point x is one of the nodes that belong to the element, $K(k)$ behaves like $\log|x-y|$, as $|x-y| \to 0$. The integral of the singular part is taken analytically, and quadrature is applied to the regular part. In addition to number of elements and order of Gaussian quadrature, a third factor which determines accuracy is the numerical integration scheme used in calculating the Green's functions. Simpson's rule is found to yield satisfactory accuracy in these calculations. Tables I–V present the results of the numerical tests applied to determine how the accuracy is influenced by the parameters—number of integration points used in Simpson's rule of integration, order of Gaussian quadrature and number of elements. Tables VI–IX compare the present procedure with the results of previous works.[1,2,7,15]

The Fourier inversion integrals in equation (13) are calculated for rings of Stokeslets with radius $r(y) = 0{\cdot}1, 0{\cdot}3, 0{\cdot}6$ and $z' = 0{\cdot}1, 0{\cdot}4$ and $0{\cdot}9$ for velocities at $r_0 = 1$ and $z = 0$. Important parameters of the Simpson's rule are N = number of integration points and T = upper limit of integration (replacing infinity in the Fourier integrals). Four different groups of values of these parameters are considered: (A) $N = 200$, $I = 50$, (B) $N = 400$, $T = 50$, (C) $N = 600$, $T = 50$ and (D) $N = 200$, $T = 25$. Results of different choices are tabulated in Table I. Comparison with exact results shows that the error in almost all cases is less than 0·005% when z is small and less than 0·01% when z is close to unity. Table I indicates that decreasing the size of the subdivisions from 0·25 to 0·125 substantially improves the results. However, taking $T = 25$ instead of 50 (a choice that will reduce the processing time by a factor of two) does not effect the accuracy so much.

Table III. λ_U and λ_V for several values of order of Gaussian quadrature m ($T = 25{\cdot}0$, $N = 200$, $n_e = 10$ for all cases)

	$a/r_0 = 0{\cdot}5$		$a/r_0 = 0{\cdot}7$	
m	λ_U	λ_V	λ_U	λ_V
1	5·8727	4·9678	22·630	16·359
3	5·9400	4·9847	24·253	17·128
4	5·9411	4·9857	24·267	17·138
5	5·9416	4·9861	24·275	17·144

Table IV. For a fixed number of integration points ($m \times n_e$) using higher order Gaussian quadratures improves the accuracy of λ_U faster than increasing number of elements

	$a/r_0 = 0{\cdot}5$		$a/r_0 = 0{\cdot}7$	
n_e	$m = 1$	$m = 5$	$m = 1$	$m = 5$
10	$\lambda_U = 5{\cdot}873$	5·942	22·63	24·28
18	5·912	5·946	23·82	24·62
28	5·921	5·947	24·06	24·66
48	5·928	5·948	24·23	24·68

Table V. Improvement of results by increasing n_e = number of subdivisions for fixed values of the other parameters, $N = 100$, $T = 25{\cdot}0$ $m = 5$

	$a/r_0 = 0{\cdot}5$		$a/r_0 = 0{\cdot}7$	
n_e	λ_U	λ_V	λ_U	λ_V
10	5·9439	4·9881	24·380	17·217
14	5·9474	4·9935	24·649	17·433
18	5·9486	4·9953	24·723	17·495
28	5·9495	4·9967	24·773	17·538
38	5·9497	4·9971	24·786	17·549
48	5·9498	4·9972	24·791	17·553

Table VI. Comparison of present results (obtained by using $N = 200$, $T = 25{\cdot}0$ $m = 5$, $n_e = 28$) with the results of Leichtberg *et al.*,[7] Tözeren[2] and Wang *et al.*[1]

	Leichtber *et al.*						Present	
a/b	λ_U	λ_V	Tözeren		Wang *et al*		results	
0·1	1·263	1·255	1·263	1·255	1·263	1·255	1·263	1·255
0·2	1·680	1·636	1·680	1·635	1·680	1·635	1·680	1·635
0·3	2·373	2·231	2·371	2·229	2·370	2·229	2·370	2·229
0·4	3·599	3·223	3·593	3·216	3·592	3·216	3·591	3·216
0·5	5·973	5·017	5·952	4·999	5·949	4·996	5·947	4·995
0·6	11·20	8·696	11·11	8·627	11·10	8·617	11·09	8·611
0·7	25·29	17·91	24·77	17·54	24·70	17·49	24·66	17·45

Table VII. Comparison of various spheroidal particle solutions (Chen and Skalak's[16] solutions are for particle spacing of three particle diameters), where δ is the ratio of the axial to radial thickness of the spheroid

δ	Chen and Skalak[16]		Wakiya[15]		Present results	
1·414	2·762	2·597	2·717	2·554	2·779	2·613
0·943	2·298	2·163	2·302	2·164	2·317	2·179

Table VIII. λ_U and λ_V for a pair of spheres, $a/r_0 = 0{\cdot}3$ and particle spacing $2\beta a$

β	1·001	1·005	1·01	2	3	4	5
λ_U	1·948	1·950	1·953	2·306	2·367	2·370	2·370
λ_V	1·823	1·825	1·828	2·166	2·266	2·229	2·229

The alternative to numerical integration for Green's function is contour integration and residue calculation in the complex plane. Although its formulation is simple and straightforward no program of comparable efficiency to numerical integration could be developed because of the following difficulties: (1) neither the series nor the asymptotic formulae are suitable for computing Bessel functions in some intermediate range of the complex variable, and (2) the number of residues to be calculated for satisfactory accuracy increases rapidly for small values of $x_3(=z)$.

Further information on different choices of T and N is presented in Table II. The variables tabulated for various T and N are drag coefficients $\lambda_U = \text{drag}/(6\pi\mu aU)$ and $\lambda_V = \text{drag}/(6\pi\mu aV)$. The number of elements, n_e, in all the cases, was equal to 10. The results are given for a/r_0 (ratio of particle diameter to tube diameter) $= 0{\cdot}5$ and $0{\cdot}7$. The change in λ_U (or λ_V) from $N = 400$ to 600 is approximately 40 times smaller than the change from $N = 200$ to 400. This shows that the results for $N = 600$ may be considered as converged at least up to five digits. Very good accuracy compared to converged results is obtained by $N = 200$ and $T = 25$ (four significant figures for $a/r_0 \leq 0{\cdot}5$ and an error less than 0·05 per cent for $a/r_0 = 0{\cdot}7$).

The results presented in Table III show that λ_U changes little for order of Gaussian quadrature, m, greater than 3. Significantly more accurate results (for $N = 200$, $T = 50$, $n_e = 10$) are obtained by increasing m from 1 to 3. This conclusion is important because $m = 1$ actually corresponds to the assumption that traction is constant within each element. The improvement is, therefore, due to our use of higher order interpolation (linear) for tractions. Table IV compares λ_U for $a/r_0 = 0{\cdot}5$ and different values of m and n_e. With $m = 1$, $n_e = 48$ (total number of integration points = 48) error is much greater than $m = 5$, $n_e = 10$ (number of integration points = 50). This is further evidence that type of interpolation used for traction strongly affects the accuracy.

Another series of numerical experiments are carried out, as shown in Table V to study convergence of λ_U as a function of n_e. In all cases $T = 25$, $N = 100$, $m = 5$. For $\lambda = 0{\cdot}5$ continuity of four figures and results accurate to 0·07 per cent for $\lambda = 0{\cdot}7$ are obtained at $n_e = 28$.

Table IX. Comparison of λ_U and λ_V for a pair of spheres given by Leichtberg *et al.*[7] with the present results (β = particle spacing)

	Leichtberg *et al.*[7]		Present results		
a/r_0	β	λ_U	λ_V	β	λ_U	λ_V
0·3	1·0	2·076	1·920	1·001	1·948	1·823
	2·0	2·320	2·117	2·0	2·306	2·166
0·5	1·0	5·656	4·911	1·001	5·496	4·575
	2·0	5·968	4·988	2·0	5·937	4·983
0·7	1·0	24·41	17·46	1·001	24·05	16·92
	2·0	25·28	17·50	2·0	24·60	17·40

Results of previous works on spherical particles[1,2,7] are compared with the present results in Table VI. The values of the parameters were $T=25{\cdot}0$, $N=200$, $n_e=28$, $m=5$. This choice yields convergence of four figures in λ for $a/r_0 \leq 0{\cdot}5$. A small error is introduced in λ by using these values for $a/r_0 \geq 0{\cdot}5$. The magnitude of this error can be accurately predicted by using Tables I–V. Table VI shows a good agreement between the results of Tözeren,[2] Wang and Skalak[1] and the present work, but a marked difference between Leichtberg *et al.*[7] and the others. Especially, the disagreement between Leichtberg *et al.*[7] and Tözeren[2] is unexpected, because both use the same numerical procedure: the boundary method based on solutions of Stokes equations, series in spherical co-ordinates and integral transforms in cylindrical. Studying the interactions of an infinite chain of spheres, Wang and Skalak[1] use series in spherical and cylindrical co-ordinates. It is very unlikely that the three completely different approaches of Wang and Skalak,[1] Tözeren[2] and the present work (based on the boundary integral equation method) are in error by almost the same amount.

Table VII compares some spheroidal particle results. Chen and Skalak's[16] solutions presented in this Table are for an infinite chain of spheroids with β = particle spacing $=6a$. Increasing the number of particles in the chain, and decreasing the spacing, reduces the coefficient of additional drag. This can be seen by comparing Chen and Skalak's[16] solutions with present results for a single spheroid given in Table VII. Also given in this table are single spheroid solutions by Wakiya.[15] The accuracy of his solutions is not satisfactory, especially in the case of prolate spheroids.

In Table VIII the λ_U and λ_V for a pair of spheres with $a/r_0=0{\cdot}3$ are given for several values of β = particle spacing. The number of elements, $n_e=14$ leads to converged results for $a/r_0=0{\cdot}3$. This Table shows that the drag for touching spheres is substantially lower than for single spheres. However, for $\beta>4a$ (and $a/r_0=0{\cdot}3$) particles in the chain have little influence on each other.

Finally, Table IX compares the present results on a pair of spheres with the results of Leichtberg *et al.*[7] (see Table 4 of their work). According to their results, λ_V is very little affected by variations in particle spacing especially for larger values of a/r_0. This is in contradiction with the results of Wang and Skalak[1] on an infinite chain of spheres. Moreover, the disagreement between present results and those of Leichtberg *et al.*[7] (see Table VI) is more obvious in this case of a pair of spheres. Some error is introduced in our results by using only 14 elements for each sphere (see Table V). This error is less than 0·1 per cent for $0{\cdot}3<a/r\leq 0{\cdot}5$ and 0·5 per cent for $a/r_0>0{\cdot}5$. But the discrepancies are larger than these figures, as can be seen from Table IX.

CONCLUSIONS

The applications presented above demonstrate that the boundary integral equation method used in the solution of Stokes problems in tubes is superior to boundary methods and the method of reflections because it is independent of particle shapes and to finite elements and finite differences because no formulation of these for arbitrary chains has been developed yet. Currently work is in progress studying flows of chains of particles shaped like white and red blood cells in capillaries using the formulation given in this paper.

ACKNOWLEDGEMENTS

This work has been supported by the Turkish Scientific Research Council and NATO as project no. MAG 559 and RG110.80.

REFERENCES

1. H. Wang and R. Skalak, *J. Fluid Mech.*, **38,** 75–96 (1969).
2. H. Tözeren, 'Torque on eccentric spheres flowing in tubes', *J. App. Mech.*, **49,** 279–283.
3. J. Happel and H. Brenner, *Low Reynolds number Hydrodynamics*, Prentice Hall, New York, 1965.
4. H. Lamb, *Hydrodynamics*, Dover, 1932.
5. M. Stimson and G. B. Jeffery, *Proc. Roy. Soc., Series A*, **111,** 110 (1926).
6. A. Tözeren and R. Skalak, *J. Fluid Mech.*, **82,** 289–339 (1977).
7. S. Leichtberg, R. Preffer and S. Weinbaum, *Int. J. Multiphase Flow*, **3,** 147–169 (1976).
8. O. C. Zienkiewicz, D. W. Kelly and P. Bettess, *Int. J. Num. Meth. Eng.*, **11,** 355–375 (1977).
9. G. K. Youngren and A. Acrivos, *J. Fluid Mechanics*, **69,** (2), 337–403 (1975).
10. M. A. Jaswon and A. R. Ponter, *Proc. Roy. Soc. Series A*, **273,** 237–246 (1963).
11. T. A. Cruse, 'Numerical solutions in three dimensional elastostatics', *Int. J. Solids Structures*, **5,** 1259–1274 (1969).
12. N. Liron and R. Shahar, *J. Fluid Mechanics*, **86,** (4), 727–744 (1978).
13. O. A. Ladyzhenskaya, *The Mathematical Theory of Viscous Incompressible Flow*, Gordon and Breach, New York, 1969.
14. C. A. Brebbia and S. Walker, *Boundary Element Techniques in Engineering*, Butterworths, London, 1979.
15. S. Wakiya, *J. Phys. Soc. Japan*, **12,** 1130 (1957).
16. T. C. Chen and R. Skalak, *Appl. Scient. Res.*, **22,** 403–441 (1970).